Nanoscale Horizons

ROYAL SOCIETY OF CHEMISTRY

COMMUNICATION

View Article Online
View Journal | View Issue

Check for updates

Cite this: *Nanoscale Horiz.*, 2026, 11, 254

Received 24th March 2025,
Accepted 2nd October 2025

DOI: 10.1039/d5nh00178a

rsc.li/nanoscale-horizons

Antibacterial properties and underlying mechanisms of $Mo_2TiC_2T_x$ and $Mo_2Ti_2C_3T_x$ MXenes targeting *Escherichia coli* (Gram-negative bacterium)

Mohsen Pilevar,[a] Mostafa Dadashi Firouzjaei, *[a] Anupma Thakur, [b] B. S. Nithin Chandran,[b] Sara Wahib,[c] Delanie Williams,[a] Hesam Jafarian,[a] Carolina Bryant,[d] Annabelle Bedford, [b] Adriana Riveros,[a] Qiaoli Liang, [e] Khaled A. Mahmoud,[c] Mark Elliott *[a] and Babak Anasori*[bf]

The widespread use of antibiotics has led to an increased number of antimicrobial-resistant (AMR) pathogens, highlighting the need for novel antibacterial nanomaterials with chemical and structural tunability. Here, we present the antibacterial properties/pathways of two molybdenum-based double transition metal (DTM) MXenes ($Mo_2TiC_2T_x$ and $Mo_2Ti_2C_3T_x$) and compare them with $Ti_3C_2T_x$ MXene. We demonstrate that the antibacterial effectiveness of these MXenes is concentration- and time-dependent, with prolonged exposure time being more influential at lower concentration levels (<25 µg mL^{-1}). Physical damage to *E. coli* cell walls by MXene nanoknives (sharp edges of MXene flakes), and disruption in metabolic functions through oxidative stress were key antibacterial pathways for $Mo_2TiC_2T_x$, $Mo_2Ti_2C_3T_x$, and $Ti_3C_2T_x$ MXenes. A 1 h sonication of MXene solutions reduced their flake sizes (average lateral size of 234 ± 163 nm) and led to substantial improvement of their antibacterial performance by bolstering the availability of nanoknives for physical damage to bacterial cells. However, prolonged sonication (2 h) resulted in reduced antibacterial effectiveness, potentially due to morphological defects of MXene flakes. We also studied the metal ion release and disc inhibition zone, which revealed no direct correlation between the MXenes' antibacterial properties and the leaching of ions or fragments. This study demonstrates the potential for improving the antibacterial effectiveness of molybdenum-containing DTM MXenes by controlling their chemical and structural characteristics.

New concepts

This study presents the first comprehensive investigation of molybdenum-containing double-transition metal (DTM) MXenes—$Mo_2TiC_2T_x$ and $Mo_2Ti_2C_3T_x$—as antibacterial agents. While previous reports primarily focused on mono-transition metal MXenes (*e.g.*, $Ti_3C_2T_x$), this work reveals new structure–function relationships governing the antibacterial efficacy of Mo-based DTM MXenes. We demonstrate that nanoknife-enabled physical disruption of bacterial membranes is the dominant antibacterial mechanism, and that performance is significantly enhanced by flake size reduction through optimized sonication. Importantly, we decouple the contributions of oxidative stress and metal ion release, finding them to be negligible compared to physical interactions. These insights provide a critical step forward in understanding how compositional and morphological parameters influence the biocidal behavior of 2D materials, enabling the rational design of next-generation MXene-based antibacterial coatings and therapeutic platforms.

Introduction

Antibiotics are widely used for treating microbial infectious diseases.[1] However, pathogens are increasingly showing resistance to the most commonly used antibiotics due to the rise of drug-resistant microorganisms.[2] It's projected that by 2050, antimicrobial resistance (AMR) will lead to 10 million fatalities annually, with associated costs of approximately $100 trillion.[3] Hence, there is an urgent need for new approaches to combat AMR pathogens.

Nanomaterial-based therapeutics have gained a lot of interest as they can be inherently biocidal, serve as carriers for antibacterial agents, or offer both functionalities.[4] They can be utilized to overcome such infections by hindering the development of AMR bacteria,[5,6] simultaneous delivery of multiple antimicrobial agents,[7] and precise delivery of antimicrobial drugs to the infection site.[8] The physicochemical properties (*e.g.*, surface chemistry, particle/flake size, and morphology) of

---

[a] Department of Civil, Construction, and Environmental Engineering, University of Alabama, Tuscaloosa, AL, 35487, USA. E-mail: mdfirouzjaei@ua.edu, melliott@eng.ua.edu
[b] School of Materials Engineering, Purdue University, West Lafayette, 47907 IN, USA. E-mail: banasori@purdue.edu
[c] Qatar Environment and Energy Research Institute (QEERI), Hamad Bin Khalifa University, Qatar Foundation, P.O. Box 34110, Doha, Qatar
[d] Department of Chemical and Biological Engineering, University of Alabama, Tuscaloosa, AL, 35487, USA
[e] Department of Chemistry and Biochemistry, University of Alabama, Tuscaloosa, AL, 35487, USA
[f] School of Mechanical Engineering, Purdue University, West Lafayette, 47907 IN, USA

nanostructured materials can also influence their interactions with bacterial cells and consequently their antibacterial properties.[9,10] Hence, utilizing nanostructured materials with tunable structure-composition properties could further bolster their effectiveness in therapeutic applications. In this regard, MXenes, an emerging class of two-dimensional (2D) materials, are an attractive choice for therapeutic and biomedical applications due to their structural tunability and functionality.[11–13]

MXenes can include one or more types of 3d–5d block transition metals of groups 3–6 of the periodic table interleaved with carbon and/or nitrogen.[14] The antibacterial properties of mono-transition metal (mono-M) MXenes, 2D metal carbides/nitrides with only one type of transition metal (*e.g.*, $Ti_3C_2T_x$), have been studied in recent years.[15–18] Direct physical damage to bacterial cell walls by sharp edges of MXene flakes, termed "nanoknives", and disruption in bacterial metabolic functions through oxidative stress have been reported as their primary antibacterial mode-of-action.[15] The antibacterial effectiveness of mono-M MXenes (*e.g.*, $Ti_3C_2T_x$, Nb_2CT_x) can also be affected by their structural and morphological characteristics, dispersibility, and surface charges.[16,18,19] To the best of our knowledge, there has been only one study on the antibacterial properties of double-transition metal (DTM) MXenes (with two different transition metals in their structure), specifically those containing Ti and V in their structure (*i.e.*, $TiVCT_x$).[20] However, there is no study on the antibacterial properties of DTM MXenes that contain molybdenum in their structures. Mo-containing DTM MXenes are of special interest because Mo ions, when integrated into nanostructured materials (*e.g.*, MoS_2, MoO_x), can induce antibacterial properties by promoting oxidative stress and disrupting the metabolic functions of bacterial cells.[21,22] Moreover, the integration of Mo ions in antibacterial pharmaceuticals can improve their stability while reducing the mammalian cytotoxicity levels associated with the antibacterial metal nanoparticles.[23,24]

In this study, the antibacterial properties of two Mo-containing DTM MXenes, namely $Mo_2TiC_2T_x$ and $Mo_2Ti_2C_3T_x$, were investigated and compared with $Ti_3C_2T_x$. Various antibacterial tests and characterizations were utilized to: (1) quantify and compare the antibacterial performance of Mo-containing DTM ($Mo_2TiC_2T_x$ and $Mo_2Ti_2C_3T_x$) with mono-M ($Ti_3C_2T_x$) MXenes, (2) investigate the impact of MXenes' structural and morphological characteristics on their antibacterial effectiveness, and (3) elucidate the potential antibacterial modes-of-action for $Mo_2TiC_2T_x$ and $Mo_2Ti_2C_3T_x$ MXenes. *Escherichia coli* (*E. coli*) was used as a representative Gram-negative bacterium due to its well-characterized physiology and extensive use as a model organism in microbiological and antibacterial studies.

Results and discussion

MXene synthesis and characterization

The unique crystal structure of $Ti_3C_2T_x$, $Mo_2TiC_2T_x$, and $Mo_2Ti_2C_3T_x$ MXenes (Fig. 1a) can influence their physicochemical properties, including their antibacterial effectiveness. The XRD patterns for $Ti_3C_2T_x$, $Mo_2TiC_2T_x$, and $Mo_2Ti_2C_3T_x$ MXenes and their corresponding MAX phases are shown in Fig. 1b. The MAX phase peaks[25,26] disappeared upon synthesis of $Ti_3C_2T_x$, $Mo_2TiC_2T_x$, and $Mo_2Ti_2C_3T_x$ MXene films. Since these MXene films were made by filtration of their delaminated single-flake nanosheets colloidal suspension (and not multilayer powders), only the 00L peaks are detected in the XRD patterns. We used delaminated single-flake nanosheets in our study to maximize the benefit from the large surface area of MXene flakes and their interactions with bacteria. The exact peak location and their corresponding peaks, along with the *d*-spacing calculated from the 00L peak position of the MAX and MXene XRD patterns, are provided in Table S1. Notably, the illustrated broadening and downshift in MAX phases' peaks indicate an increase in their *d*-spacing, due to the removal of the A-layer and the presence of intercalated water or cations between the MXene sheets.[25] Furthermore, the scanning electron microscopy (SEM) images demonstrate the bulk morphology of MAX phases (Fig. 1c), and the 2D structure of delaminated flakes of $Ti_3C_2T_x$, $Mo_2TiC_2T_x$, and $Mo_2Ti_2C_3T_x$ MXenes (Fig. 1d). The energy-dispersive X-ray (EDX) mapping analyses of $Ti_3C_2T_x$, $Mo_2TiC_2T_x$, and $Mo_2Ti_2C_3T_x$ MXenes further confirmed the elemental composition and uniform distribution of elements in the synthesized MXenes (Fig. S1 and Table S2). After confirming the successful synthesis of delaminated MXenes, we used them for our antibacterial experiments.

Antibacterial performance assessment *via* growth-inhibition tests

A series of concentration- and time-dependent growth-inhibition tests were conducted to investigate the antibacterial efficacy of mono-M (*i.e.*, $Ti_3C_2T_x$) and Mo-containing DTM MXenes (*i.e.*, $Mo_2TiC_2T_x$ and $Mo_2Ti_2C_3T_x$) against *E. coli* as a Gram-negative bacterium (Materials and methods in SI). Growth-inhibition tests were initially carried out using phosphate-buffered saline (PBS) as the suspension medium due to its suitability for the preservation and growth of bacterial cells.[27] The colloidal MXene suspensions exhibited minimal antibacterial efficacy (inhibition efficiency (IE) $< 5\%$) even at the concentration of 100 $\mu g\ mL^{-1}$ (Fig. S2). The visual appearance of colloidal suspensions hinted at potential MXene agglomeration inside the PBS solution, likely due to electrostatic and van der Waals interactions between MXenes' functional groups and dissociated ions in the buffer solution, as reported in similar antibacterial studies of 2D materials.[28,29] Therefore, modified growth-inhibition experiments were designed by replacing PBS with deionized (DI) water to promote uniform dispersion of MXene flakes. The hydrophilic nature of detected (Fig. S3) terminal groups (–F, Ti–O, and Mo–O) in $Ti_3C_2T_x$, $Mo_2TiC_2T_x$, and $Mo_2Ti_2C_3T_x$ MXenes can promote the dispersibility of their flakes in DI water.[30]

The modified growth-inhibition tests were carried out at different concentrations (5, 10, 25, 50, and 100 $\mu g\ mL^{-1}$) of $Ti_3C_2T_x$, $Mo_2TiC_2T_x$, and $Mo_2Ti_2C_3T_x$ MXenes. All samples showed under 35% inhibition efficiency (IE) at the concentration of 5 $\mu g\ mL^{-1}$ (Fig. S4). Increasing the MXene concentration to 10 $\mu g\ mL^{-1}$ (Fig. 2a) resulted in $<15\%$ changes in IEs

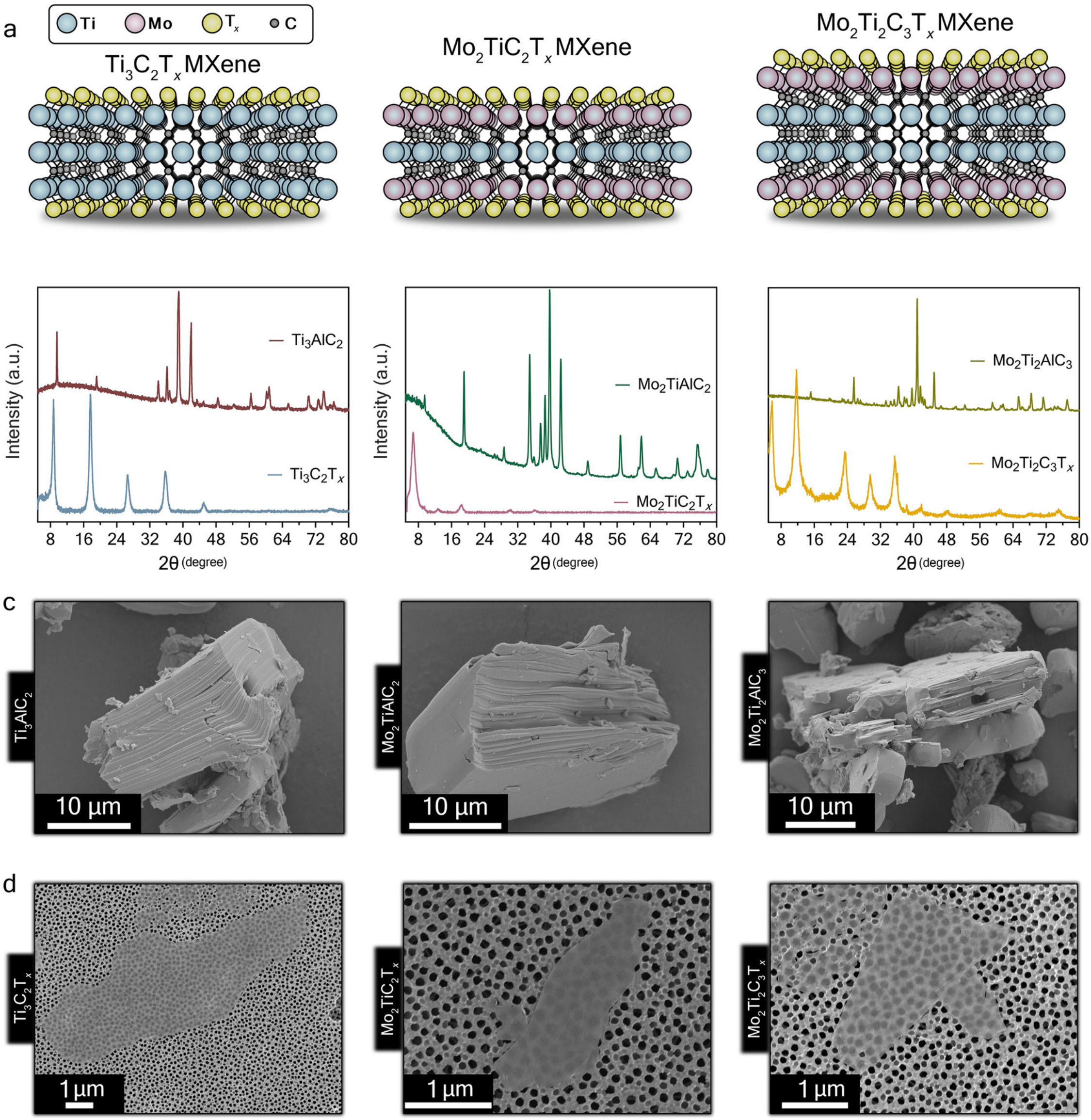

Fig. 1 (a) Schematic of the molecular structure of $Ti_3C_2T_x$, $Mo_2TiC_2T_x$, and $Mo_2Ti_2C_3T_x$ MXenes, (MXenes' terminal groups, Ti, Mo, and C atoms are shown as yellow, blue, red, and gray spheres, respectively) (b) XRD spectra of $Ti_3C_2T_x$, $Mo_2TiC_2T_x$, and $Mo_2Ti_2C_3T_x$ MXenes and their corresponding MAX phases, (c) SEM images of Ti_3AlC_2, Mo_2TiAlC_2, and $Mo_2Ti_2AlC_3$ MAX phases, and (d) SEM images of $Ti_3C_2T_x$, $Mo_2TiC_2T_x$, and $Mo_2Ti_2C_3T_x$ flakes after delamination. The molecular structure of Mo-containing DTM MXenes is comprised of layers of Mo sandwiched between Ti layers, while $Ti_3C_2T_x$ MXene contains layers of only Ti. The synthesis of $Ti_3C_2T_x$, $Mo_2TiC_2T_x$, and $Mo_2Ti_2C_3T_x$ MXenes was verified by their characteristic peaks, along with the disappearance of MAX phases' peaks in their corresponding XRD pattern. Electron-transparent thin flakes under SEM show successful etching and delamination of MAX phases.

even after 2 h of contact time. However, extending the exposure time to 3 h led to a major improvement of IEs, at 75.3%, 65.4%, and 61.5% for $Ti_3C_2T_x$, $Mo_2TiC_2T_x$, and $Mo_2Ti_2C_3T_x$ MXenes, respectively. Additionally, increasing the concentration of MXenes (≥ 25 µg mL^{-1}) greatly enhanced their antibacterial performance while requiring shorter exposure times (Fig. 2b–d). For instance, at 25 µg mL^{-1} (Fig. 2b) and only after 1 h of exposure time, $Ti_3C_2T_x$, $Mo_2TiC_2T_x$, and $Mo_2Ti_2C_3T_x$ MXenes obtained IEs of 92.2%, 89%, and 86.2%, respectively. By increasing the concentration to 100 µg mL^{-1} of MXene, $Ti_3C_2T_x$, $Mo_2TiC_2T_x$, and $Mo_2Ti_2C_3T_x$ obtained IEs of 76.7%, 83.9%, and 80.9%, respectively, immediately upon exposure to the *E. coli* cells (Fig. 2d). The growth-inhibition results indicated that both concentration and exposure time of MXenes substantially affect the antibacterial effectiveness of $Ti_3C_2T_x$, $Mo_2TiC_2T_x$, and $Mo_2Ti_2C_3T_x$ MXenes. Notably, prolonged exposure time was more effective at lower MXene concentrations (<25 µg mL^{-1}). The low IEs observed for the tested MXenes at low concentrations (<25 µg mL^{-1}) may be attributed to electrostatic repulsion between the negatively charged surfaces of both *E. coli* cells and MXene flakes.[18] The zeta potential measurements of $Ti_3C_2T_x$ (−43.3 mV), $Mo_2TiC_2T_x$ (−30.0 mV), and $Mo_2Ti_2C_3T_x$ (−31.0 mV) (Fig. S5) confirmed the negatively charged surface of these MXene nanosheets, further supporting the proposed mechanism. Table S3

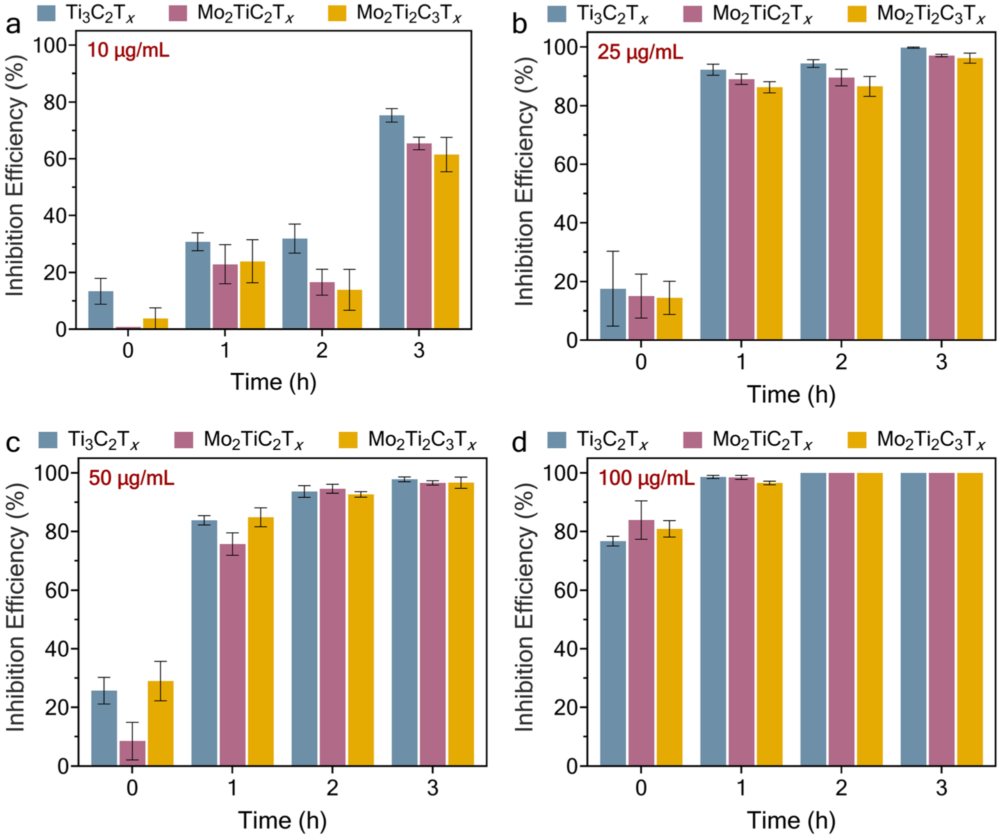

Fig. 2 Concentration- and time-dependent antibacterial performance of $Ti_3C_2T_x$, $Mo_2TiC_2T_x$, and $Mo_2Ti_2C_3T_x$ MXenes examined *via* modified growth-inhibition tests at (a) 10 μg mL^{-1}, (b) 25 μg mL^{-1}, (c) 50 μg mL^{-1}, and (d) 100 μg mL^{-1} of MXenes against *E. coli* suspension with an initial bacterial concentration of $\sim 10^6$ CFU mL^{-1}. Both increasing MXene concentrations and prolonging the exposure time resulted in improved antibacterial performances while exposure time played an essential role at lower concentrations of MXenes (<25 μg mL^{-1}).

presents our statistical analysis of the modified growth-inhibition data of MXene concentration, exposure time, and their interaction term on their overall antibacterial efficacy. The analyses also showed that the overall antibacterial performance of the three studied MXenes was comparable and not significantly different. We next investigated various antibacterial pathways to elucidate the findings from the modified growth-inhibition results.

Effects of sonication on antibacterial performance of MXenes

To investigate the nanoknives' effects on MXenes' antibacterial properties, we probe sonicated the MXene solutions for 1 h as a pretreatment step, to reduce their flake sizes and increase the exposed MXene edges. It is known that subjecting MXenes colloidal suspension to sonication reduces the lateral sizes while inducing minimal chemical alterations.[31] After the 1-h sonication step, we conducted a time-dependent growth-inhibition test at fixed MXene concentrations of 10 μg mL^{-1} (Materials and methods in SI). The antibacterial performance of sonicated MXenes (Fig. 3a) was substantially improved compared to untreated samples (Fig. 2a). Notably, sonicated $Ti_3C_2T_x$, $Mo_2TiC_2T_x$, and $Mo_2Ti_2C_3T_x$ MXenes achieved IEs above 98% (Fig. 3a) after 2 h of exposure time, whereas the untreated samples (Fig. 2a) only achieved IEs of 31.8%, 16.9%, and 13.9%, respectively. We measured the average MXene flake lateral sizes before and after 1 h sonication (Fig. 3b and Fig. S6 and S7). Before sonication, the average lateral flake size of untreated $Ti_3C_2T_x$ was measured to be 2823 ± 287 nm, while 631 ± 280 and 895 ± 400 nm were obtained for $Mo_2TiC_2T_x$ and $Mo_2Ti_2C_3T_x$, respectively. After 1 h of sonication, flake sizes were reduced across all samples with $Ti_3C_2T_x$, $Mo_2TiC_2T_x$, and $Mo_2Ti_2C_3T_x$ MXenes, obtaining an average flake size of 231 ± 142, 229 ± 183, and 242 ± 165 nm, respectively. The substantial size reduction in $Ti_3C_2T_x$ flakes can be attributed to their initial large lateral sizes compared to $Mo_2TiC_2T_x$ and $Mo_2Ti_2C_3T_x$ MXenes. It has been shown that MXenes with lateral sizes of a few μm are more susceptible to mechanical fragmentation under sonication[31] compared to submicron flake sizes. The results suggest that the enhanced antibacterial performance of sonicated MXenes can be attributed to the reduced lateral sizes of their flakes, as more contact sites (edges) were available for direct physical damage to the bacterial cell walls.[16]

The mass density of the studied MXenes is another critical factor influencing the availability and effectiveness of their flakes. To better assess this, the theoretical densities of $Ti_3C_2T_x$, $Mo_2TiC_2T_x$, and $Mo_2Ti_2C_3T_x$ MXenes were calculated alongside the estimated number of available flakes for each MXene at the same concentration of 10 μg mL^{-1} (after 1 h of sonication). Because of the lower theoretical density of $Ti_3C_2T_x$ (ranging from 4.2 to 4.5 g cm^{-3}), there

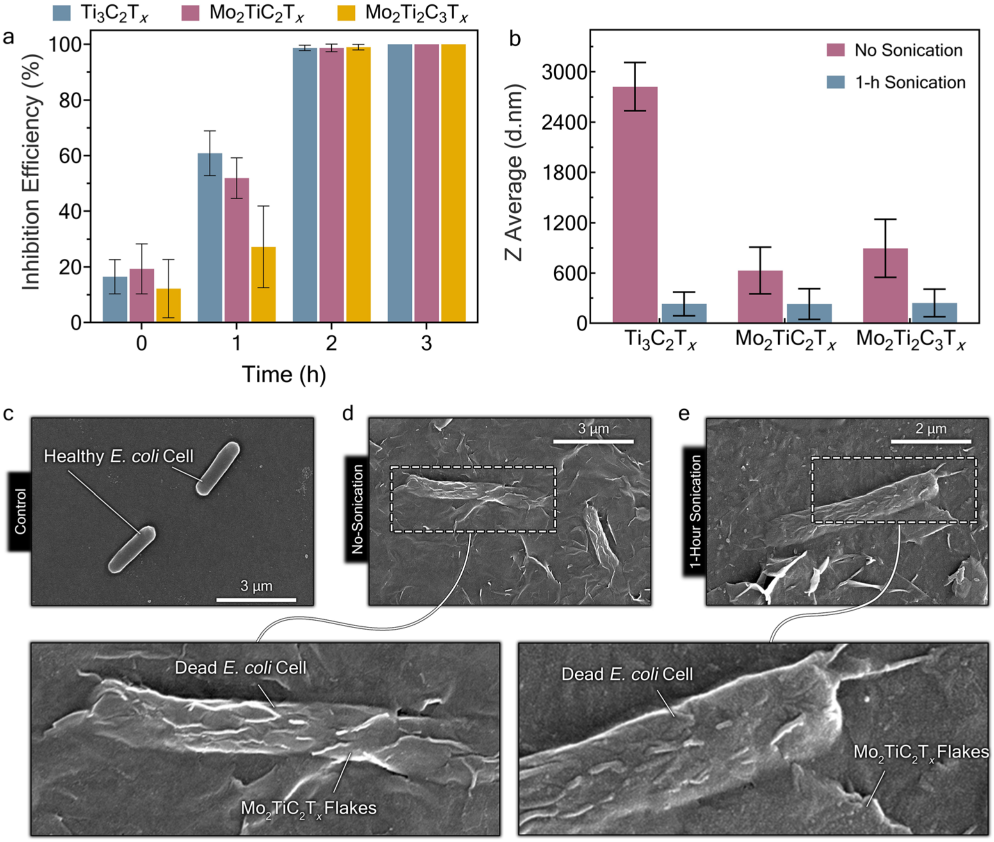

Fig. 3 (a) Time-dependent growth-inhibition performance of 1 h probe sonicated $Ti_3C_2T_x$, $Mo_2TiC_2T_x$, and $Mo_2Ti_2C_3T_x$ MXenes, (b) The average lateral size of flakes for untreated and 1 h sonicated $Ti_3C_2T_x$, $Mo_2TiC_2T_x$, and $Mo_2Ti_2C_3T_x$ MXenes obtained from dynamic light scattering (DLS) measurements, (c) SEM image of viable *E. coli* cells after incubation in the absence of colloidal $Mo_2TiC_2T_x$ MXenes, (d) morphological characteristics of a damaged *E. coli* cell after 3 h of exposure to untreated $Mo_2TiC_2T_x$ MXenes at an initial concentration of 10 μg mL^{-1}, and (e) morphological characteristics of a damaged *E. coli* cell after 3 h of exposure to 1 h sonicated $Mo_2TiC_2T_x$ MXenes. As shown in the SEM images, the morphological characteristics of viable *E. coli* cell envelopes were drastically different compared to the damaged cells. The direct physical cell damage by MXenes' nanoknives is apparent in the SEM images obtained for both untreated and sonicated samples, highlighting their importance in the antibacterial mode-of-action for $Mo_2TiC_2T_x$ MXenes, particularly in suspension modes.

are more $Ti_3C_2T_x$ MXene flakes compared to the heavier M-containing MXenes, $Mo_2TiC_2T_x$, and $Mo_2Ti_2C_3T_x$ with densities in the range of 6.1 to 6.8 g cm^{-3} (Table S4). For example, in 1 mL of a MXene solution at 10 μg mL^{-1}, we estimated 1.5 to 2 times more $Ti_3C_2T_x$ MXene flakes $(\sim 4.79 \pm 0.14) \times 10^{10}$ flakes per mL compared to $Mo_2TiC_2T_x$ and $Mo_2Ti_2C_3T_x$ with $(3.19 \pm 0.06) \times 10^{10}$ and $(2.3 \pm 0.04) \times 10^{10}$ flakes per mL, respectively. This agrees with the higher IE (60.8%) of the sonicated $Ti_3C_2T_x$ MXene after 1 h of exposure time compared to $Mo_2TiC_2T_x$ and $Mo_2Ti_2C_3T_x$ MXenes. It also agrees with the slightly lower IEs for $Mo_2Ti_2C_3T_x$ compared to $Mo_2TiC_2T_x$. The relatively thicker $Mo_2Ti_2C_3T_x$ MXene (1.2 nm for $Mo_2Ti_2C_3T_x$ *vs.* 0.9 nm for $Ti_3C_2T_x$ and $Mo_2TiC_2T_x$) with the additional atomic layer in its flake structure can limit the availability of $Mo_2Ti_2C_3T_x$ nanoknives for physical contact with bacterial cells. Therefore, these findings suggest physical cell damage by "nanoknives" as one of the primary antibacterial mode-of-action for $Ti_3C_2T_x$, $Mo_2TiC_2T_x$, and $Mo_2Ti_2C_3T_x$ MXenes, causing structural compromise and cytoplasmic leakage, which eventually leads to cell death.

The size-dependent antibacterial efficacy of $Ti_3C_2T_x$ MXenes was further explored by extending the sonication duration to 2 h, followed by a time-dependent growth-inhibition test. After 2 h of exposure to *E. coli* cells (Fig. S7a), $Ti_3C_2T_x$ MXenes showed a lower IE (17.4%) compared to 1-h sonicated samples (with an IE of 98.6%). The reduced antibacterial effectiveness of $Ti_3C_2T_x$ MXenes by extending the sonication treatment (from 1 h to 2 h) suggests that there may be optimal morphological characteristics necessary for effective penetration of the cell membrane by MXene flakes. Longer sonication (2 h of probe sonication) could cause damage to MXene flakes and could even lead to localized oxidation,[31–33] although our scanning electron microscopy (SEM) images (Fig. S7b) and transmission electron microscopy (see next section) did not show any evidence of oxidation or detectable damage. Additionally, prolonged probe sonication of MXenes has also been reported to turn MXene flakes into quantum dots (<10 nm) with rounded edges. These potential damages and sharp edge reduction could diminish the availability and effectiveness of nanoknives.[34–36] Overall, the lower bactericidal effectiveness of MXenes suggests the flake nanoknives may be compromised by 2 h probe sonication.

The morphologies of both viable and damaged *E. coli* cells were also investigated *via* SEM imaging after collecting samples from growth-inhibition tests (Materials and methods in SI). Fig. 3c demonstrates *E. coli* cells after 3 h of incubation in the absence of colloidal $Mo_2TiC_2T_x$ MXenes. The intact cellular cytoplasmic structure of the *E. coli* cells is indicative of healthy and viable conditions. Fig. 3d and e illustrate damaged *E. coli* cells alongside the sharp edges of $Mo_2TiC_2T_x$ MXene flakes. The distinct morphological alteration in the cells can infer partial rupture of the cell wall, leading to the outflow of cell contents and the ultimate lysis of bacterial cells.[16] Additional morphological characterizations of damaged *E. coli* cells, after exposure to $Ti_3C_2T_x$ and $Mo_2Ti_2C_3T_x$ MXenes, are provided in Fig. S8.

Effects of oxidative stress induced by MXenes

To further investigate the antibacterial effects of untreated and sonicated $Mo_2TiC_2T_x$ and $Mo_2Ti_2C_3T_x$ MXenes beyond membrane disruption, it is crucial to consider additional mechanisms like oxidative stress. Glutathione (GSH), a tripeptide containing a thiol group, acts as a key cellular antioxidant in bacteria, helping to maintain intracellular oxidative balance and protect cells from external electrophilic compounds.[17] The oxidation of GSH, commonly used to indicate oxidative stress from nanomaterials, including MXenes, was measured here using Ellman's assay with untreated and sonicated $Mo_2TiC_2T_x$ and $Mo_2Ti_2C_3T_x$ across concentrations of 10–100 μg mL^{-1} with incubation times of 2 and 4 hours (Materials and methods in SI). Oxidative stress mechanisms generally include ROS-mediated pathways, where reactive oxygen species (ROS) such as superoxide, hydrogen peroxide, and alkyl hydroperoxides induce cellular damage, and ROS-independent pathways, where cellular structures are directly oxidized, as seen in graphene toxicity studies.[17]

After 2 h of incubation with $Mo_2TiC_2T_x$ MXene, the GSH oxidation levels were relatively close (glutathione loss of ∼50 ± 3%) across different concentrations with or without the sonication treatment (Fig. 4a). However, after 4 h of incubation, a notable increase in GSH oxidation level was recorded for the 1 h sonicated $Mo_2TiC_2T_x$ samples with the highest GSH loss (74.8%) achieved by 100 μg mL^{-1} MXenes (Fig. 4b). Additionally, extended sonication treatments (*i.e.*, 2 h sonication time) resulted in minimal changes in the GSH oxidation levels (glutathione loss of ∼50 ± 4%) compared to untreated $Mo_2TiC_2T_x$ MXenes across all conditions (Fig. 4b). This suggests that while sonication initially enhances GSH oxidation by $Mo_2TiC_2T_x$ MXene, prolonged sonication may lead to stabilization or reduction in oxidation rates over time.

After 2 h of incubation with $Mo_2Ti_2C_3T_x$ MXene, the GSH oxidation levels showed minimal improvement across all concentrations and sonication conditions, with the highest GSH loss (37.8%) obtained by the 1 h sonicated samples at a concentration of 100 μg mL^{-1} (Fig. 4c). However, after 4 h of incubation, an increase in GSH oxidation (glutathione loss of 44.5%) was observed by 100 μg mL^{-1} of the 2 h sonicated $Mo_2Ti_2C_3T_x$ MXenes (Fig. 4d). This suggests that prolonged sonication, when coupled with extended incubation time, enhances the oxidative stress induced by $Mo_2Ti_2C_3T_x$ MXenes.

The GSH oxidation results highlight the importance of concentration, incubation time, and sonication duration on the oxidative stress induced by $Mo_2TiC_2T_x$ and $Mo_2Ti_2C_3T_x$ MXenes. While higher MXene concentrations and extended incubation times resulted in slight to moderate improvements in their GSH oxidation levels, the impact of the sonication duration was not as straightforward. Notably, the highest GSH losses (%) were obtained using different sonication durations for each MXene type, namely 1 h sonication for $Mo_2TiC_2T_x$ and 2 h sonication for $Mo_2Ti_2C_3T_x$ MXenes. The statistical significance

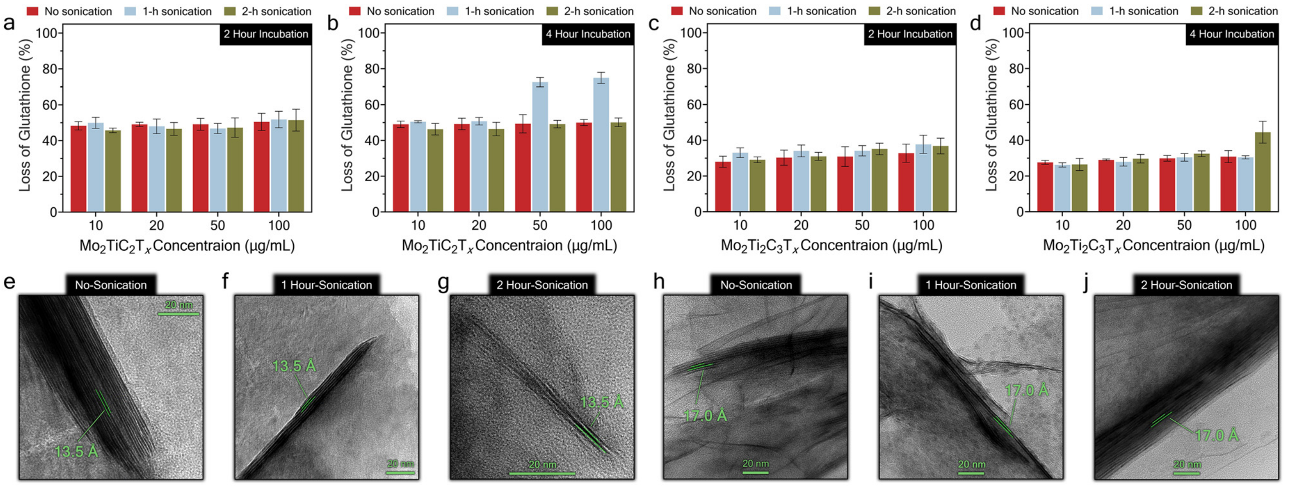

Fig. 4 Concentration- and time-dependent evaluation of glutathione loss (%) induced by (a) $Mo_2TiC_2T_x$ after 2 h of incubation (b) $Mo_2TiC_2T_x$ after 4 h of incubation, (c) $Mo_2Ti_2C_3T_x$ after 2 h of incubation, and (d) $Mo_2Ti_2C_3T_x$ after 4 h of incubation. The interlayer spacing was measured for (e) untreated $Mo_2TiC_2T_x$, (f) 1 h sonicated $Mo_2TiC_2T_x$, (g) 2 h sonicated $Mo_2TiC_2T_x$, (h) untreated $Mo_2Ti_2C_3T_x$, (i) 1 h sonicated $Mo_2Ti_2C_3T_x$, (j) 2 h sonicated $Mo_2Ti_2C_3T_x$. The optimal sonication duration varied by MXene type, with 1 h sonication resulting in the highest glutathione oxidation levels for $Mo_2TiC_2T_x$, and 2 h sonication being most effective for $Mo_2Ti_2C_3T_x$ MXenes. Additionally, the sonication treatment did not alter the interlayer spacing of $Mo_2TiC_2T_x$ and $Mo_2Ti_2C_3T_x$ MXenes. Hence, no meaningful relationship was observed between the interlayer spacing of $Mo_2TiC_2T_x$ and $Mo_2Ti_2C_3T_x$ MXenes and their oxidative stress properties.

of the variables (*i.e.*, MXene concentration, exposure time, and sonication duration) on the GSH oxidation results was further investigated *via* a general linear model (Tables S5 and S6). Additionally, sonication treatment has been reported to improve the oxidative stress of Nb-containing mono-M MXenes (Nb_2CT_x and $Nb_4C_3T_x$) by increasing the interlayer spacing between their flakes.[16] However, TEM imaging of untreated (Fig. 4e), 1 h sonicated (Fig. 4f), and 2 h sonicated (Fig. 4g) $Mo_2TiC_2T_x$ MXenes showed no difference between their interlayer spacing, suggesting that the distance between flakes is not directly related to the oxidative stress posed by $Mo_2TiC_2T_x$ MXenes. Similar to $Mo_2TiC_2T_x$ MXene, the sonication treatment did not affect the interlayer spacing between $Mo_2Ti_2C_3T_x$ flakes (Fig. 4h–j). Overall, it can be inferred from Fig. 2 and 4a–d that oxidative stress, induced by $Mo_2TiC_2T_x$ and $Mo_2Ti_2C_3T_x$ MXenes, had minimal contribution to their bactericidal properties. Additionally, the minimal differences in GSH oxidation levels between untreated and sonicated samples suggest that potential surface chemistry alterations, such as nano-titania (TiO_2) formation, had limited impacts on the antibacterial properties of $Ti_3C_2T_x$, $Mo_2TiC_2T_x$, and $Mo_2Ti_2C_3T_x$ MXenes under normal light conditions.[37]

Metal ion release and disc inhibition assessment

The cumulative concentrations of the released metal ions (Ti and/or Mo) from untreated and 1 h sonicated $Ti_3C_2T_x$, $Mo_2TiC_2T_x$, and $Mo_2Ti_2C_3T_x$ were measured to investigate their potential relationship with the antibacterial properties of the mentioned MXenes (Materials and methods in SI). For untreated $Mo_2TiC_2T_x$ and $Mo_2Ti_2C_3T_x$ MXenes, the majority of Mo ions were released within the first hour of suspension, reaching concentrations of 3.64 and 0.92 μg mL^{-1}, respectively (Fig. 5a). Minimal variation in the cumulative concentrations was recorded afterward (suspension time >1 h), with measured Mo concentrations of 3.87 and 1.01 μg mL^{-1} after 3 h of suspension for $Mo_2TiC_2T_x$ and $Mo_2Ti_2C_3T_x$, respectively. The 1-h sonication treatment resulted in increased concentrations of the released Mo ions from both $Mo_2TiC_2T_x$ and $Mo_2Ti_2C_3T_x$ MXenes, with the highest cumulative concentrations reaching 5.71 μg mL^{-1} and 3.58 μg mL^{-1}, respectively (Fig. 5b). As previously shown in Fig. 2a, prolonging the exposure times from 1 h to 3 h resulted in 42.6% and 37.59% improvement in IEs obtained by untreated $Mo_2TiC_2T_x$ and $Mo_2Ti_2C_3T_x$ MXenes, respectively. Similarly, we recorded 46.8% and 71.7%

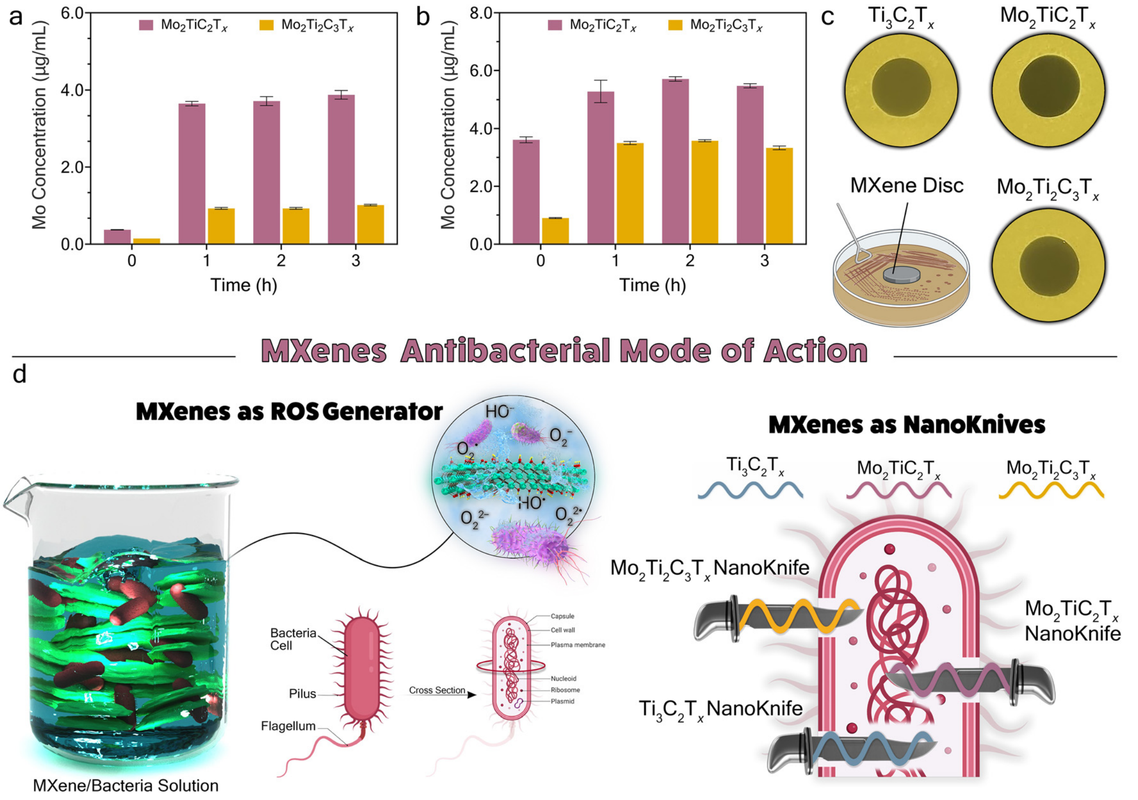

Fig. 5 Time-dependent release of Mo ion from 10 μg mL^{-1} colloidal suspensions of (a) untreated $Mo_2TiC_2T_x$ and $Mo_2Ti_2C_3T_x$ MXenes, (b) 1 h sonicated $Mo_2TiC_2T_x$ and $Mo_2Ti_2C_3T_x$ MXenes, (c) Disc inhibition zone tests using membrane coupons previous coated with colloidal suspensions of $Ti_3C_2T_x$, $Mo_2TiC_2T_x$, and $Mo_2Ti_2C_3T_x$ MXenes. (d) Schematic of antibacterial mode-of-action for $Ti_3C_2T_x$, $Mo_2TiC_2T_x$, and $Mo_2Ti_2C_3T_x$ MXenes. 1-h sonication treatment increased the amount of released Mo ions from both $Mo_2TiC_2T_x$ and $Mo_2Ti_2C_3T_x$ MXenes. No meaningful relationship was observed between the time-dependent antibacterial performance of the mentioned MXenes (at 10 μg mL^{-1}) and the cumulative concentrations of released Mo ions. The absence of inhibition zones around the MXene-coated coupons suggests that the antibacterial properties governed by oxidative stress and the release of antibacterial agents are hindered under static conditions. The schematic illustrates the important roles of nanoknives and oxidative stress in the overall antibacterial effectiveness of $Ti_3C_2T_x$, $Mo_2TiC_2T_x$, and $Mo_2Ti_2C_3T_x$ MXenes.

improvement in IEs for the sonicated samples when the exposure time was extended from 1 h to 2 h (Fig. 3a). The notable improvement in their antibacterial performance did not correlate with the observed trends of the cumulative concentrations of Mo ions, released from $Mo_2TiC_2T_x$ and $Mo_2Ti_2C_3T_x$ suspensions (Fig. 5a and b). Hence, it can be inferred that the released Mo ions were unlikely to play a crucial role in the overall antibacterial effectiveness of $Mo_2TiC_2T_x$ and $Mo_2Ti_2C_3T_x$ MXenes.

Similar to Mo ions, no meaningful correlation was observed between the cumulative concentration of released Ti ions and the antibacterial efficacy of untreated and sonicated $Mo_2TiC_2T_x$ and $Mo_2Ti_2C_3T_x$ MXenes (Fig. S9). In addition, an analogous trend was observed in the concentration of released Ti ions from untreated $Ti_3C_2T_x$ MXene, negating any potential correlation with previously reported IEs (Fig. 2a). The 1-h sonication treatment facilitated the release of Ti ions from $Ti_3C_2T_x$, resulting in a high concentration of 5.73 $\mu g\ mL^{-1}$ measured after 1 h of suspension. This might suggest a potential relationship between released Ti ions and the high IE (61.0%) obtained by sonicated $Ti_3C_2T_x$ MXene after 1 h of exposure time (Fig. 3a). However, minimal changes in released Ti ions were observed thereafter (suspension time >1 h), while the IE increased from 61.0% to 99.0% by extending the exposure time from 1 h to 2 h (Fig. 3a). Hence, it can be inferred that released Ti ions were not significantly influential in the overall antibacterial efficacy of $Ti_3C_2T_x$ MXene. This was consistent with the reported bioinert properties of Ti ions and nanoparticles like nano-titania (TiO_2).[38,39] A comparative illustration of the cumulative concentrations of released metal ions and antibacterial performance of untreated and 1 h sonicated MXenes is further depicted in Fig. S10.

The antibacterial mode-of-action of mono-M ($Ti_3C_2T_x$) and Mo-containing DTM MXenes ($Mo_2TiC_2T_x$, and $Mo_2Ti_2C_3T_x$) was further investigated *via* disc inhibition zone tests under a static mode (Materials and methods in SI). No apparent inhibitory zone was formed around the membrane coupons, coated with colloidal suspensions of $Ti_3C_2T_x$, $Mo_2TiC_2T_x$, and $Mo_2Ti_2C_3T_x$ MXenes (Fig. 5c). While the absence of an inhibition zone does not necessarily negate the antibacterial properties of tested MXenes, it highlights the structural stability of MXene sheets with minimal diffusion of potential antibacterial agents (*e.g.*, leaching metal ions) under static conditions. In addition, the absence of inhibitory zones infers a substantial reduction in the antibacterial effectiveness of the tested MXenes, which can be due to the restricted effects of MXene nanoknives under static mode.

Conclusion

In summary, we showed that the antibacterial effectiveness of $Ti_3C_2T_x$, $Mo_2TiC_2T_x$, and $Mo_2Ti_2C_3T_x$ MXenes against *E. coli* depends on both concentration and duration of exposure, with longer exposure times being particularly influential at lower concentration levels ($<25\ \mu g\ mL^{-1}$). Notably, at 25 $\mu g\ mL^{-1}$ and 1 h of exposure, all tested MXenes exhibited IE $>$ 85%, identifying this as the lowest concentration that effectively inhibited bacterial growth across all samples. Further, ultrasonic-assisted experiments revealed that MXenes' antibacterial mode-of-action is highly dependent on the size and morphology of the flakes (*i.e.*, nanoknives), and by reducing the flake sizes (with an optimum sonication duration), their efficacy increases due to more exposed flake edges. Additional tests (GSH loss, ion release, and disc inhibition zone tests) elucidated that oxidative stress can minimally contribute to their antibacterial efficacy, while no conclusive relationship was observed between the release of antibacterial agents (*e.g.*, leaching metal ions) from MXenes' structure and their antibacterial properties.

We summarized our proposed antibacterial pathways for $Ti_3C_2T_x$, $Mo_2TiC_2T_x$, and $Mo_2Ti_2C_3T_x$ in Fig. 5d, with nanoknives and oxidative stress as their most likely antibacterial modes-of-action. The nanoknives played an important role in the overall antibacterial effectiveness of MXenes, with their impact highly affected by their size and morphology. Notably, a 1-h sonication treatment of all tested MXenes resulted in flakes with reduced sizes (234 ± 163 nm), leading to substantially improved antibacterial efficacy due to the enhanced availability of nanoknives. However, prolonged sonication treatments (2 h) substantially reduced their antibacterial effectiveness, further highlighting the importance of nanoknives' morphological characteristics for effective physical damage to bacterial cells. The exact relationship between the structural and morphological characteristics of nanoknives and their biocidal properties can be further studied for different classes of MXenes and other 2D materials. Also, given the high release concentration of Ti ions from MXenes and their bioinert properties, future studies can focus on the potential of MXenes for precise drug delivery to infection sites.

Experimental section

Materials

Trypticase soy broth (TSB), agar, phosphate buffer saline (PBS), and *Escherichia coli* (*E. coli*, ATCC 35695) were used in the antibacterial experiments. Glutaraldehyde ($C_5H_8O_2$ $>99\%$), osmium tetroxide (OsO_4 $>99\%$), $Na_2HPO_4{\cdot}7H_2O$, $NaH_2PO_4{\cdot}H_2O$, and ethanol ($>99\%$) were purchased from Sigma-Aldrich and used for the preparation of cell-MXenes samples prior to scanning electron microscopy (SEM) imaging. 0.02-micron aluminum oxide membranes were purchased from Sterlitech and used as the substrate for the SEM samples. 0.2-micron PVDF filters were purchased from MilliporeSigma and used in the disc inhibition zone tests. In addition, 0.1 μm Supor filters were purchased from Pall Corporation and employed to separate metal ions from impurities before ion concentration measurements (*via* ICP-OES) in metal ion release tests. Tris Hydrochloride, 5,5′-dithio-bis (2-nitrobenzoic acid) (DTNB), and Hydrogen peroxide solution were purchased from – and used in oxidative stress measurements by Ellman's assay.

MXene synthesis and characterization

The synthesis and characterization of $Ti_3C_2T_x$, $Mo_2TiC_2T_x$, and $Mo_2Ti_2C_3T_x$ MXenes, along with their respective MAX phases, were carried out following established protocols (Materials and methods in SI).[25,26,40,41] X-ray diffraction (XRD) measurements, field-emission scanning electron microscopy (FESEM), and high-resolution transmission electron microscopy (HR-TEM) were further utilized to characterize the synthesized MXenes (Materials and methods in SI).

Antibacterial assessment experiments

The antibacterial performance of $Ti_3C_2T_x$, $Mo_2TiC_2T_x$, and $Mo_2Ti_2C_3T_x$ MXenes was evaluated through a series of concentration- and time-dependent cell growth-inhibition tests. For this purpose, *Escherichia coli* (*E. coli*), as a model Gram-negative bacterium, was cultivated in the trypticase soy broth (TSB) at 37 °C overnight and sub-cultured to obtain the culture suspensions for the antibacterial experiments. 4 mL of the sub-cultured medium was then centrifuged at 6000 rpm (Multifuge X1R Centrifuge, Thermo Fisher Scientific, USA) for 5 minutes and repeatedly pelletized with PBS to remove any remaining macromolecules and growth medium components. The resultant pellet cells were then diluted with sterile deionized (DI) water to achieve the cell concentration of approximately 10^6 CFU mL^{-1}, determined through optical density measurements at 600 nm wavelength (OD_{600}). The concentration-dependent antibacterial performance of MXenes was assessed by using 5, 10, 25, 50, and 100 μg mL^{-1} of mono-M ($Ti_3C_2T_x$) and DTM ($Mo_2TiC_2T_x$ and $Mo_2Ti_2C_3T_x$) MXenes. For this purpose, previously prepared MXene stock solutions were diluted accordingly and added to *E. coli* suspension (10^6 CFU mL^{-1}) to achieve the desired final concentrations. Then, the samples were incubated at 37 °C under 200 rpm shaking speed for 3 h. The bacterial concentration of samples was measured *via* the standard colony-forming unit (CFU) method at 1 h time intervals to evaluate the time-dependent antibacterial performance of the MXenes. To achieve this, 100 μL of serially diluted samples were plated on the solidified agar plates and put in the incubator (37 °C) for approximately 20 h. Colonies grown on each plate were then counted and used to calculate the bacterial concentration of each sample. Suspension of *E. coli* culture (10^6 CFU mL^{-1}) in DI water (with no MXenes) was used as the control. Finally, the antibacterial performance of the samples was evaluated by calculating the inhibition efficiency (IE%) using the following equation:

$$\mathrm{IE}(\%) = \left(1 - \frac{N_\mathrm{S}}{N_\mathrm{C}}\right) \times 100 \tag{1}$$

where N_S and N_C are the bacterial concentrations (CFU mL^{-1}) in MXene-treated and control samples, respectively. All experiments were conducted in triplicates and the average bacterial concentrations were used in IE (%) calculations.

The antibacterial properties of MXenes were further assessed *via* various experiments such as probe sonication pretreatment, oxidative stress induced by MXenes, cumulative release of metal ions, and disc inhibition zone experiments (Materials and methods in SI).

Conflicts of interest

There are no conflicts to declare.

Data availability

The data supporting the findings of this study are available from the corresponding author upon reasonable request. Due to file size and institutional repository limitations, the datasets—including raw antibacterial assay data, characterization files (SEM, TEM, XRD), and image analyses—will be provided *via* direct email communication.

Supplementary information (SI) is available. See DOI: https://doi.org/10.1039/d5nh00178a.

Acknowledgements

This research benefited greatly from funding provided by USDATAT-RWTS 00–69526, USEPA Cooperative Agreement MX-00D87019, The Richard Lounsbery Foundation, and the Transforming Wastewater Infrastructure in the United States project of Columbia World Projects. USDA or other agencies have not formally reviewed this paper, and the views expressed in this document are solely those of the authors and do not necessarily reflect those of the agencies. A. T., A. B., B. S. N. C. and B. A. acknowledge the support of the US National Science Foundation award number CMMI-2134607.

References

1 S. Marzouk, D. Nguyen and C. Sabet, Reviving antibiotic power, *Nat. Rev. Chem.*, 2024, 1.
2 S. J. Lam, *et al.*, Combating multidrug-resistant Gram-negative bacteria with structurally nanoengineered antimicrobial peptide polymers, *Nat. Microbiol.*, 2016, **1**(11), 1–11.
3 J. O'Neill, *Tackling drug-resistant infections globally: final report and recommendations*. 2016.
4 P. Makvandi, *et al.*, Metal-based nanomaterials in biomedical applications: antimicrobial activity and cytotoxicity aspects, *Adv. Funct. Mater.*, 2020, **30**(22), 1910021.
5 D. O. Schairer, *et al.*, The potential of nitric oxide releasing therapies as antimicrobial agents, *Virulence*, 2012, **3**(3), 271–279.
6 K. Blecher, A. Nasir and A. Friedman, The growing role of nanotechnology in combating infectious disease, *Virulence*, 2011, **2**(5), 395–401.
7 L. Zhang, *et al.*, Development of nanoparticles for antimicrobial drug delivery, *Curr. Med. Chem.*, 2010, **17**(6), 585–594.
8 J. G. Leid, *et al.*, In vitro antimicrobial studies of silver carbene complexes: activity of free and nanoparticle carbene formulations against clinical isolates of pathogenic bacteria, *J. Antimicrob. Chemother.*, 2012, **67**(1), 138–148.
9 F. Cao, *et al.*, Defect-rich adhesive nanozymes as efficient antibiotics for enhanced bacterial inhibition, *Angew. Chem., Int. Ed.*, 2019, **58**(45), 16236–16242.
10 L. Zhang, *et al.*, Nature-inspired construction of MOF@ COF nanozyme with active sites in tailored microenvironment and pseudopodia-like surface for enhanced bacterial inhibition, *Angew. Chem., Int. Ed.*, 2021, **60**(7), 3469–3474.

11 B. C. Wyatt, *et al.*, Alkali cation stabilization of defects in 2D MXenes at ambient and elevated temperatures, *Nat. Commun.*, 2024, **15**(1), 6353.

12 K. Huang, *et al.*, Two-dimensional transition metal carbides and nitrides (MXenes) for biomedical applications, *Chem. Soc. Rev.*, 2018, **47**(14), 5109–5124.

13 L. M. Dong, *et al.*, Two-dimensional metal carbides and nitrides (MXenes): preparation, property, and applications in cancer therapy, *Nanophotonics*, 2020, **9**(8), 2125–2145.

14 B. C. Wyatt, *et al.*, Design of Atomic Ordering in Mo2Nb2C3T x MXenes for Hydrogen Evolution Electrocatalysis, *Nano Lett.*, 2023, **23**(3), 931–938.

15 A. Arabi Shamsabadi, *et al.*, Antimicrobial mode-of-action of colloidal $Ti_3C_2T_x$ MXene nanosheets, *ACS Sustainable Chem. Eng.*, 2018, **6**(12), 16586–16596.

16 R. P. Pandey, *et al.*, Effect of sheet size and atomic structure on the antibacterial activity of Nb-MXene nanosheets, *ACS Appl. Nano Mater.*, 2020, **3**(11), 11372–11382.

17 K. Rasool, *et al.*, Antibacterial activity of $Ti_3C_2T_x$ MXene, *ACS Nano*, 2016, **10**(3), 3674–3684.

18 F. Seidi, *et al.*, MXenes Antibacterial Properties and Applications: A Review and Perspective, *Small*, 2023, **19**(14), 2206716.

19 F. Perreault, *et al.*, Antimicrobial properties of graphene oxide nanosheets: why size matters, *ACS Nano*, 2015, **9**(7), 7226–7236.

20 Q. He, *et al.*, Double transition-metal TiVCTX MXene with dual-functional antibacterial capability, *Mater. Lett.*, 2022, **308**, 131100.

21 S. Roy, *et al.*, Mechanistic insight into the antibacterial activity of chitosan exfoliated MoS_2 nanosheets: membrane damage, metabolic inactivation, and oxidative stress, *ACS Appl. Bio Mater.*, 2019, **2**(7), 2738–2755.

22 J. Liao, *et al.*, Molybdenum-based antimicrobial nanomaterials: A comprehensive review, *Nano Today*, 2023, **50**, 101875.

23 L. F. Deravi, J. D. Swartz and D. W. Wright, The biomimetic synthesis of metal oxide nanomaterials, *Preface XV List of Contributors XIX*, 2009, 16.

24 U. Kadiyala, N. A. Kotov and J. S. VanEpps, Antibacterial metal oxide nanoparticles: challenges in interpreting the literature, *Curr. Pharm. Des.*, 2018, **24**(8), 896–903.

25 B. Anasori, *et al.*, Two-dimensional, ordered, double transition metals carbides (MXenes), *ACS Nano*, 2015, **9**(10), 9507–9516.

26 A. Thakur, *et al.*, Step-by-step guide for synthesis and delamination of Ti3C2Tx MXene, *Small Methods*, 2023, **7**(8), 2300030.

27 C. H. Liao and L. Shollenberger, Survivability and long-term preservation of bacteria in water and in phosphate-buffered saline, *Lett. Appl. Microbiol.*, 2003, **37**(1), 45–50.

28 S. F. Seyedpour, *et al.*, Improved performance and antifouling properties of thin-film composite polyamide membranes modified with nano-sized bactericidal graphene quantum dots for forward osmosis, *Chem. Eng. Res. Des.*, 2018, **139**, 321–334.

29 X. Zou, *et al.*, Mechanisms of the antimicrobial activities of graphene materials, *J. Am. Chem. Soc.*, 2016, **138**(7), 2064–2077.

30 S. Patra, *et al.*, Hydrophobic MXene with enhanced electrical conductivity, *Surf. Interfaces*, 2023, **39**, 102969.

31 K. Maleski, *et al.*, Size-dependent physical and electrochemical properties of two-dimensional MXene flakes, *ACS Appl. Mater. Interfaces*, 2018, **10**(29), 24491–24498.

32 M. Malaki, A. Maleki and R. S. Varma, MXenes and ultrasonication, *J. Mater. Chem. A*, 2019, **7**(18), 10843–10857.

33 A. Iqbal, *et al.*, Improving oxidation stability of 2D MXenes: synthesis, storage media, and conditions, *Nano Convergence*, 2021, **8**(1), 9.

34 G. Yang, *et al.*, Biodegradable and photostable Nb2C MXene quantum dots as promising nanofluorophores for metal ions sensing and fluorescence imaging, *Sens. Actuators, B*, 2020, **309**, 27735.

35 Q. Zhang, *et al.*, Selective detection of Fe^{3+} ions based on fluorescence MXene quantum dots *via* a mechanism integrating electron transfer and inner filter effect, *Nanoscale*, 2020, **12**(3), 1826–1832.

36 Z. Wang, *et al.*, Versatile cutting method for producing fluorescent ultrasmall MXene sheets, *ACS Nano*, 2017, **11**(11), 11559–11565.

37 D. Tobaldi, *et al.*, Silver-modified nano-titania as an antibacterial agent and photocatalyst, *J. Phys. Chem. C*, 2014, **118**(9), 4751–4766.

38 S. Qin, *et al.*, Approaches based on passive and active antibacterial coating on titanium to achieve antibacterial activity, *J. Biomed. Mater. Res. Part A*, 2018, **106**(9), 2531–2539.

39 B. Li, *et al.*, Preparation and antibacterial properties of plasma sprayed nano-titania/silver coatings, *Mater. Chem. Phys.*, 2009, **118**(1), 99–104.

40 B. Anasori, *et al.*, Mo_2TiAlC_2: A new ordered layered ternary carbide, *Scr. Mater.*, 2015, **101**, 5–7.

41 T. S. Mathis, *et al.*, Modified MAX phase synthesis for environmentally stable and highly conductive Ti_3C_2 MXene, *ACS Nano*, 2021, **15**(4), 6420–6429.